Toward P-Band Passive Microwave Sensing of Soil Moisture

Nan Ye, Jeffrey P. Walker, In-Young Yeo, Thomas J. Jackson, Yann Kerr, Edward Kim, Andrew McGrath, Ivan PopStefanija, Mark Goodberlet, and James Hills

***Abstract*— Currently, near-surface soil moisture at a global scale is being provided using National Aeronautics and Space Administration's (NASA's) Soil Moisture Active Passive (SMAP) and European Space Agency's (ESA's) Soil Moisture and Ocean Salinity (SMOS) satellites, both of which utilize L-band (1.4 GHz; 21 cm wavelength) passive microwave remote sensing techniques. However, a fundamental limitation of this technology is that the water content can only be measured for approximately the top 5-cm layer of soil moisture, and only over low-to-moderate vegetation covered areas in order to meet the 0.04 m^3/m^3 target accuracy, limiting its applicability. Consequently, a longer wavelength radiometer is being explored as a potential solution for measuring soil moisture in a deeper surface layer of soil and under denser vegetation. It is expected that P-band (wavelength of 40 cm and frequency of 750 MHz) could potentially provide soil moisture information for the top ~10-cm layer of soil, being one-tenth to one-quarter of the wavelength. In addition, P-band is expected to have higher soil moisture retrieval accuracy due to its reduced sensitivity to vegetation water content and surface roughness. To demonstrate the potential of P-band passive microwave soil moisture remote sensing, a short-term airborne field experiment was conducted over a center pivot irrigated farm at Cressy in Tasmania, Australia, in January 2017. First results showing a comparison of airborne P-band brightness temperature observations against airborne L-band brightness temperature observations and ground soil moisture measurements are presented. The P-band brightness temperature was found to have a similar but stronger response to soil moisture compared to L-band.**

***Index Terms*— Airborne field experiments, brightness temperature, L-band, P-band, soil moisture.**

Manuscript received April 15, 2019; revised September 12, 2019 and January 28, 2020; accepted February 1, 2020. This work was supported by the Australian Research Council through the Toward P-Band Soil Moisture Sensing From Space Project under Grant DP170102373, Grant LE0453434, and Grant LE150100047. *(Corresponding author: Nan Ye.)*

Nan Ye and Jeffrey P. Walker are with the Department of Civil Engineering, Monash University, Clayton, VIC 3800, Australia (e-mail: nan.ye@monash.edu).

In-Young Yeo is with the School of Engineering, The University of Newcastle, Callaghan, NSW 2308, Australia.

Thomas J. Jackson is with the Hydrology and Remote Sensing Laboratory, USDA ARS, Beltsville, MD 20705 USA.

Yann Kerr is with CNES, Center for Space Studies of the BIOsphere (CESBIO), 31401 Toulouse, France.

Edward Kim is with the NASA Goddard Space Flight Center (GSFC), Greenbelt, MD 20771 USA.

Andrew McGrath is with the College of Science and Engineering, Flinders University, Adelaide, SA 5042, Australia.

Ivan PopStefanija and Mark Goodberlet are with ProSensing Inc., Amherst, MA 01002 USA.

James Hills is with the Tasmanian Institute of Agriculture, University of Tasmania—Cradle Coast Campus, Burnie, TAS 7320, Australia.

Color versions of one or more of the figures in this letter are available online at http://ieeexplore.ieee.org.

Digital Object Identifier 10.1109/LGRS.2020.2976204

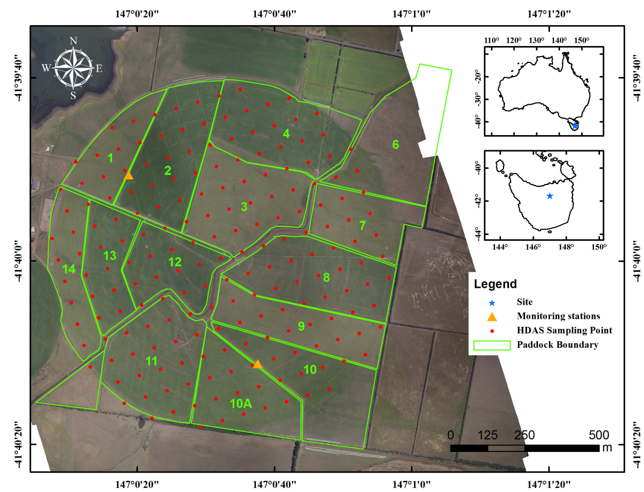

Fig. 1. Location of the study area, monitoring stations, and ground soil moisture sampling points in Cressy, Tasmania, Australia.

I. Introduction

THE first soil moisture dedicated satellite, the Soil Moisture and Ocean Salinity (SMOS) mission [1], was launched by the European Space Agency (ESA) in November 2009, and subsequently, the Soil Moisture Active Passive (SMAP) mission [2] was launched by the National Aeronautics and Space Administration (NASA) in January 2015 [3]–[5]. Due to its protected band, all-weather capability, direct relationship to soil moisture via the soil dielectric constant, and reduced sensitivity to surface roughness relative to active microwave and higher frequency passive microwave remote sensing, the L-band microwave radiometry technique has been employed for both missions to routinely measure the microwave emission from the earth and thus retrieve global soil moisture maps using radiative transfer models [6], [7]. However, the retrieved soil moisture from L-band microwave observations is limited to the top ~5-cm soil layer under medium soil moisture conditions [8], [9], and the retrieval accuracy is sensitive to the soil surface roughness and vegetation coverage, with degraded retrieval capability under dense vegetation [10]–[12].

A number of model simulation and observational studies [13]–[15] have confirmed that the observation depth of passive microwave sensors is a function of the wavelength. Accordingly, lower frequency radiometers are expected to observe a deeper layer of soil and to be less sensitive to surface roughness and overlaying vegetation [16]–[18]. Therefore, a P-band (40 cm; 750 MHz) radiometer has been built to demonstrate the potential for providing soil moisture data for

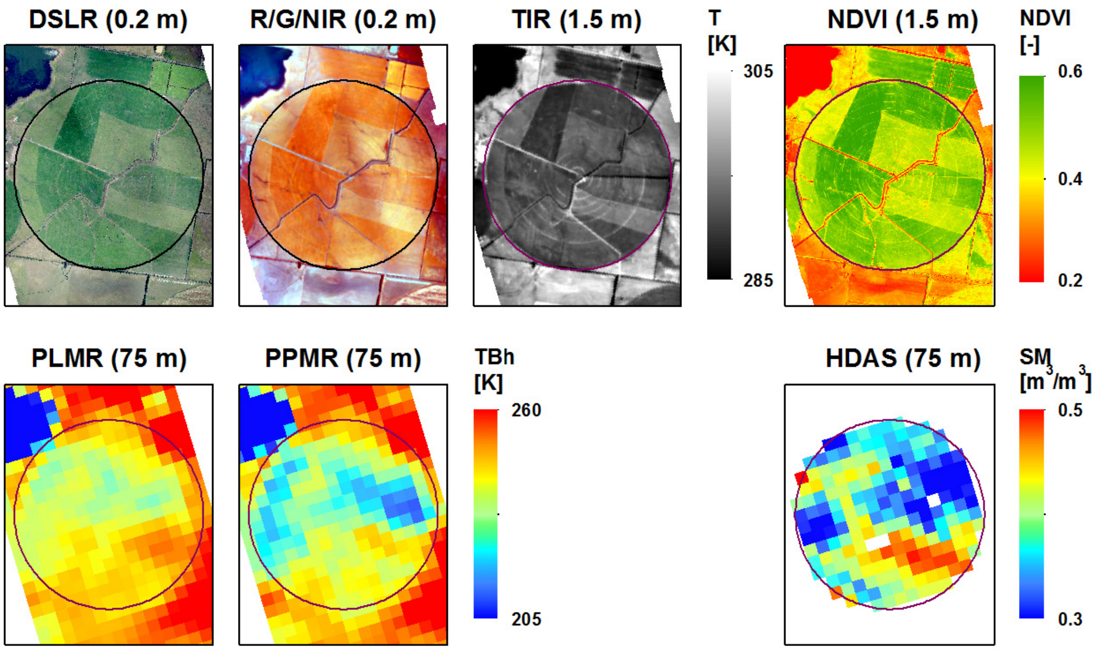

Fig. 2. Overview of airborne and ground sampling data (January 19, 2017). Brightness temperature observations of PLMR Beam 2 (22.1°) and PPMR Beam 2 (15.5°) are plotted together with optical images, derived NDVI map, and gridded ground soil moisture measurements.

TABLE I

SPECIFICATIONS OF THE AIRBORNE INSTRUMENTS

	Polarimetric P-Band Multi-beam Radiometer (PPMR)	Polarimetric L-Band Multi-beam Radiometer (PLMR)	FLIR A65	Canon EOS-5Ds Mark III	Canon EOS-1Ds Mark III
Type:	P-band microwave radiometer	L-band microwave radiometer	Thermal Infrared Camera	Digital Single Lens Reflex (DSLR) Camera	Digital Single Lens Reflex (DSLR) Camera
Frequency/ Wavelength:	742 - 752 MHz	1401 - 1425 MHz	7.5 - 13 μm	Visible (RG) and Near Infrared	Visible (RGB)
Polarization:	H & V	H & V	-	-	-
Observation Mode:	Multi-beam (linear)	Multi-beam (linear)	Snap shot (640 × 512)	Snap shot (5760 × 3240)	Snap shot (5616 × 3744)
View angle:	4 beams：±15° and ±45°	6 beams： ±7°, ±21.5° and ±38.5°	Nadir	Nadir	Nadir
Beam width:	30° × 30°	17° × 15°	44° × 36°	45° × 37°	45° × 37°
Ground resolution / Altitude:	75 m / 150 m	75 m / 225 m	~1.5 m / 400 m	~0.2 m / 400 m	~0.2 m / 400 m
Accuracy:	< 1.5 K	< 1.5 K	±5 °C	-	-

the top ∼10-cm layer of soil over more densely vegetated surfaces, with an overall improved accuracy. Note that for the same flying height, a larger antenna/aperture is required at P-band than L-band in order to maintain the same spatial resolution. While a series of tower-based and airborne field experiments is currently being conducted to further explore the potential of P-band passive microwave soil moisture remote sensing from space, this letter presents results from an initial airborne field experiment that demonstrates the potential for the approach.

II. Study Area and Data Sets

A three-day long airborne field experiment was conducted over a center pivot irrigated dairy farm, with a radius of ∼500 m at Cressy in Tasmania, Australia (Fig. 1), between January 17 and 19, 2017. The focus area was divided into 15 paddocks, which were alternately grazed by dairy cattle, resulting in diverse grass density across the paddocks. During the experiment, the center pivot irrigator was continuously spray irrigating the area from ∼2 m in front to ∼2 m behind the boom. Three types of instruments were used during the experiment including airborne sensors, monitoring stations, and the mobile Hydraprobe Data Acquisition System (HDAS [19]) sensors.

A small fixed-wing aircraft was used to carry the polarimetric P-band multibeam radiometer (PPMR), the polarimetric L-band multibeam radiometer (PLMR), a FLIR A65 thermal infrared (TIR) camera, a modified Canon EOS-5D Mark III Digital Single-Lens Reflex (DSLR) camera, and a Canon EOS-1Ds Mark III DSLR camera. Table I summarizes the specifications of the airborne instruments. The PPMR and PLMR were configured in a multiangular mode such that all of the beams were distributed along the flight line with different incidence angles including fore and aft. As a result, the elliptical footprints of the different beams have similar sizes across the track but slightly different sizes along the track. However, due to a high along track sampling rate, the oversampled PPMR and PLMR observations could be gridded at the same size as the across-track diameter of footprints. For each pixel, the gridded brightness temperature was, therefore, taken as

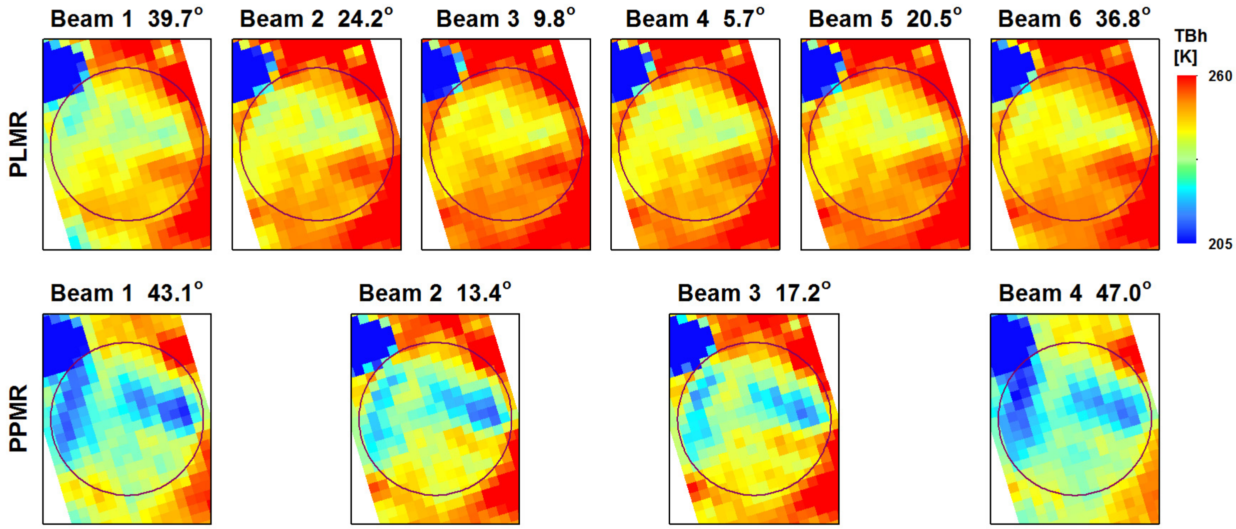

Fig. 3. (Top row) Multiangular brightness temperature maps of PLMR and (Bottom row) PPMR at horizontal polarization on January 19, 2017. Mean incidence angle over the pivot area is shown for each beam.

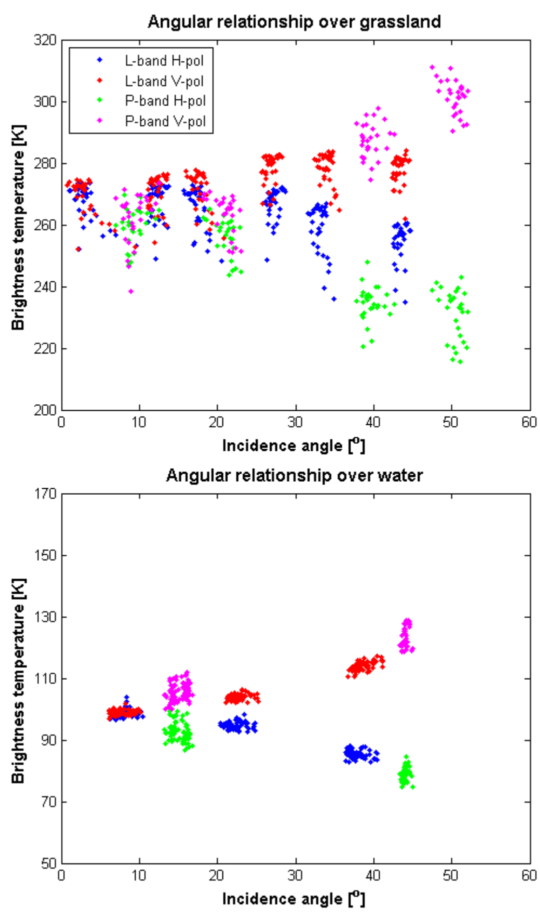

Fig. 4. (Top) Angular relationship of P- and L-band dual-polarized brightness temperature observations over a grassland area near the airport and (Bottom) water body at the northwest of the study area.

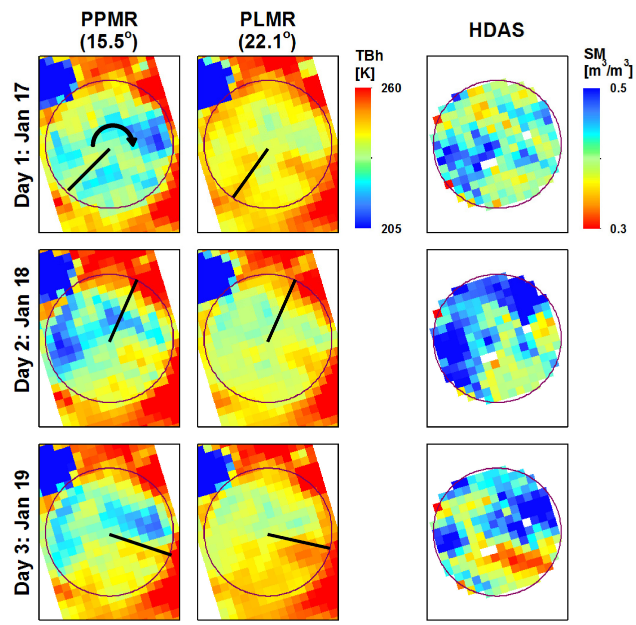

Fig. 5. Maps of P- and L-band brightness temperature observations and HDAS soil moisture measurements over the study area on three consecutive days. The black lines show the location of the center pivot irrigator during sampling with the arrow showing the direction of rotation.

the average brightness temperature of the footprints "dropped in the pixel" weighted by the reciprocal distance between the given footprint center and the pixel center. Being limited by the standard minimum permissible flying height, an across-track footprint size of ~75 m was the highest common resolution (smallest footprint) that could be achieved for PPMR and PLMR. However, this meant flying at two different altitudes due to their different fields of view. Before and after each flight, both PPMR and PLMR were removed from the aircraft and calibrated using the sky and a microwave absorber box as cold and warm targets, respectively. The FLIR A65 and the two DSLRs provided high-resolution optical images covering visible, near-infrared, and TIR spectra, collected simultaneously. All airborne data were time tagged, and georeferenced using airborne inertial navigation system (INS)/GPS records. Normalized difference vegetation index (NDVI) was calculated from airborne optical observations and plotted in Fig. 2.

Two identical monitoring stations were temporarily installed in Paddocks 2 and 10A (see Fig. 1) for the period of the experiment. These short-term monitoring stations were instrumented with a rain gauge, a TIR sensor, a leaf wetness sensor, soil moisture sensors at depths of 2.5 and 22.5 cm, and four soil temperature sensors at depths of 2.5, 5, 15, and 40 cm, in order

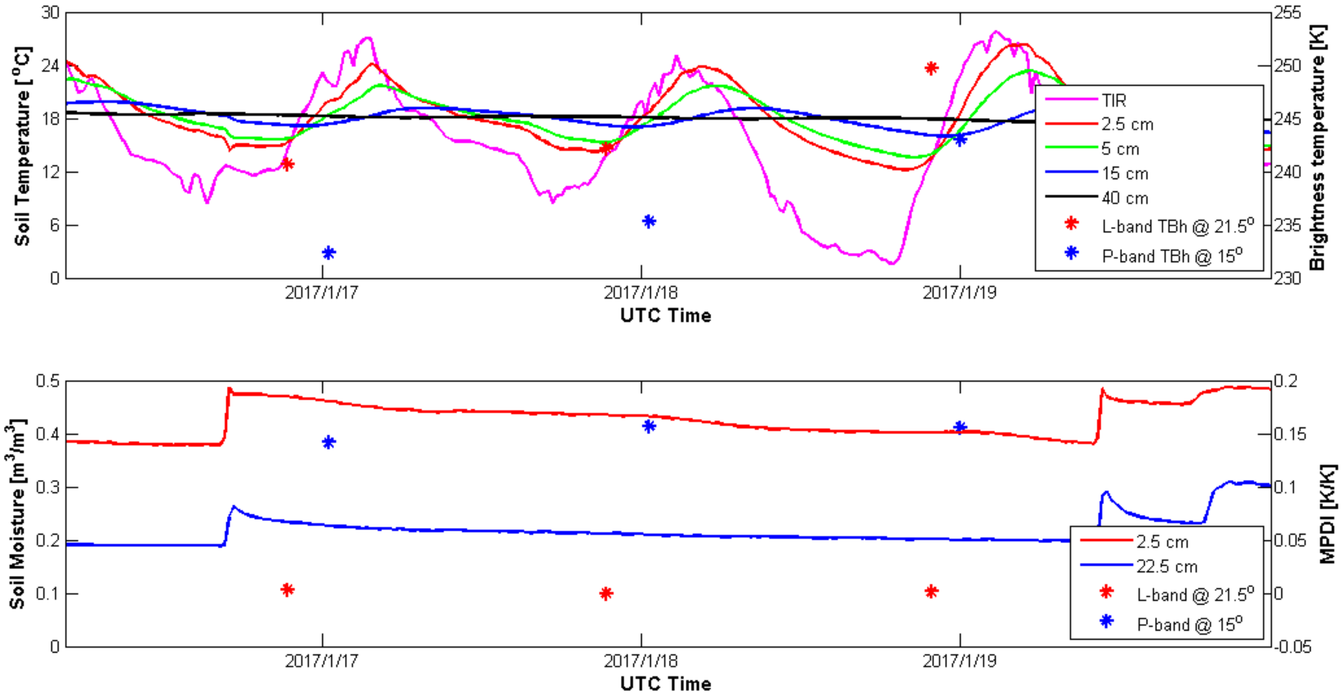

Fig. 6. (Top) Time series of TIR temperature, soil temperature at the depths of 2.5, 5, 15, and 40 cm from Paddock 10A site, together with horizontally polarized brightness temperature at L- and P-band. (Bottom) Time series of soil moisture at the depths of 2.5 and 22.5 cm, together with MPDI at L- and P-band.

to provide time series of soil moisture and soil temperature profiles. Such measurements were collected as ancillary data for soil moisture retrieval and for estimating the temporal variation of soil microwave emission during airborne sampling.

Intensive ground soil moisture sampling was carried out coincident with airborne sampling in order to obtain the spatial variability of soil moisture across the pivot irrigated dairy farm. Accordingly, 193 sampling points at 75-m spacing were arranged on a predefined grid aligned with the flight lines for ground soil moisture sampling using the HDAS. Three independent measurements of top 5-cm soil moisture were taken within an approximately 1 m radius from each HDAS sampling point, to account for sampling uncertainty and spatial heterogeneity. Subsequently, soil moisture maps were generated on the same 75-m grid of PLMR/PPMR by averaging the HDAS point-based soil moisture measurements within a radius of 75 m, in order to minimize the effect of spatial heterogeneity. Soil surface roughness and vegetation water content of representative paddocks were also measured, for the purpose of soil moisture retrieval.

III. Results

Taking airborne observations and ground measurements collected on January 19, 2017 as an example, Fig. 2 shows an overview of the field experiment data set. A number of high-resolution overlapped optical images of the farm were mosaicked, orthorectified, and georeferenced using a 3-D modeling software, while the PPMR and PLMR brightness temperature observations were georeferenced and gridded to 75-m resolution for each beam. As expected, the P-band brightness temperature map had a similar pattern to that at L-band, with both clearly showing the standing water body at the north of the farm. Fig. 3 shows PPMR and PLMR multiangular brightness temperature maps at horizontal polarization collected on January 19, 2017. Fig. 4 illustrates the dual-polarized brightness temperature observations at P- and L-bands collected over a uniform grassland (with high grass and medium soil moisture) near the airport from a low altitude, and over the water body at the northwest of the study area. Due to topographic impacts and pitch angle variation during flights, the local incidence angles of fore and aft beams of PLMR and PPMR were slightly offset while almost evenly distributed below 60°. It is clear that the P-band brightness temperature has a similar angular relationship to L-band. In addition, the angular relationship at P-band is stronger than that at L-band, especially in vertical polarization. Moreover, P-band brightness temperature at nadir is lower than that at L-band, which is expected to be a combination of higher moisture content of deeper soil layers, and less contributions from the vegetation layer and soil roughness at P-band.

Fig. 5 shows the temporal variation of brightness temperature maps at P- and L-bands together with ground soil moisture measurements during the three-day experiment. Due to the movement of the irrigator, the spatial pattern of microwave brightness temperature and soil moisture changed significantly between sampling days, especially over the freshly irrigated areas. It can be seen that both P- and L-band brightness temperatures were reduced over the northwest part of the farm between 17th and 18th January, and over the east part of the farm between 18th and 19th January, where irrigation had occurred between airborne sampling days.

During the experiment, the soil moisture ranged from 0.25 to 0.60 m^3/m^3, and vegetation water content ranged from 0.13 to 0.96 kg/m^2 across the farm. Fig. 6 shows the soil temperature and soil moisture measurements from the temporary monitoring station in Paddock 10A (see Fig. 1). The horizontally polarized brightness temperatures and microwave polarization difference index (MPDI [20]) at P- and L-bands over the station are plotted together with monitoring station data. Due to continuous irrigation and plant transpiration effects, near-surface soil moisture was significantly higher than deep soil moisture. Soil moisture in both layers was gradually decreasing with a relatively consistent offset, while the temporal changes in the brightness temperature and MPDI over this station were mainly caused by soil moisture variation and slight differences in soil temperature due to sampling time of the day. Similar trends of MPDI were found between L- and P-bands, which is potentially due to a similar sensing depths at L- and P-bands under high soil moisture conditions.

IV. Conclusion

An airborne field experiment was conducted over an irrigated dairy farm at Cressy in Tasmania, Australia, with the objectives of: 1) testing the performance of a newly developed P-band passive microwave remote sensing capability; 2) comparing P-band brightness temperature observations with L-band and ground soil moisture measurements; and 3) demonstrating the potential of the P-band passive microwave technique for soil moisture retrieval. Airborne P- and L-band brightness temperature observations collected across the three-day long field experiment, in association with high resolution optical observations and ground soil moisture sampling, showed a similar spatial pattern between P- and L-band brightness temperatures, a stronger relationship between P-band brightness temperature and incidence angle than at L-band, and a greater sensitivity of P-band brightness temperature to soil moisture. A long-term tower-based experiment and more extensive airborne field campaigns at P-band are now underway to further investigate the observation depth at P-band, impacts of surface roughness and vegetation layer on P-band brightness temperature, and the potential of P-band soil moisture sensing from space.

Acknowledgment

The authors would like to thank David McLaren from the University of Tasmania, and all the experiment participants: Ying Gao, Jon Johanson, Kiri Mason, and Jaya Pudashine.

References

[1] Y. H. Kerr *et al.*, “The SMOS mission: New tool for monitoring key elements ofthe global water cycle,” *Proc. IEEE*, vol. 98, no. 5, pp. 666–687, May 2010.

[2] D. Entekhabi *et al.*, “The soil moisture active passive (SMAP) mission,” *Proc. IEEE*, vol. 98, no. 5, pp. 704–716, May 2010.

[3] A. Al-Yaari *et al.*, “Evaluating soil moisture retrievals from ESA’s SMOS and NASA’s SMAP brightness temperature datasets,” *Remote Sens. Environ.*, vol. 193, pp. 257–273, May 2017.

[4] Y. Chen *et al.*, “Evaluation of SMAP, SMOS, and AMSR2 soil moisture retrievals against observations from two networks on the Tibetan plateau,” *J. Geophys. Res., Atmos.*, vol. 122, no. 11, pp. 5780–5792, Jun. 2017.

[5] R. Bindlish, T. J. Jackson, J. R. Piepmeier, S. Yueh, and Y. Kerr, “Intercomparison of SMAP, SMOS and aquarius L-band brightness temperature observations,” in *Proc. IEEE Int. Geosci. Remote Sens. Symp. (IGARSS)*, Jul. 2016, pp. 2043–2046.

[6] T. Mo, B. J. Choudhury, T. J. Schmugge, J. R. Wang, and T. J. Jackson, “A model for microwave emission from vegetation-covered fields,” *J. Geophys. Res.*, vol. 87, no. C13, 1982, Art. no. 11229.

[7] J.-P. Wigneron *et al.*, “L-band microwave emission of the biosphere (L-MEB) model: Description and calibration against experimental data sets over crop fields,” *Remote Sens. Environ.*, vol. 107, no. 4, pp. 639–655, Apr. 2007.

[8] M. J. Escorihuela, A. Chanzy, J. P. Wigneron, and Y. H. Kerr, “Effective soil moisture sampling depth of L-band radiometry: A case study,” *Remote Sens. Environ.*, vol. 114, no. 5, pp. 995–1001, May 2010.

[9] A. Monerris *et al.*, “Soil moisture retrieval using L-band radiometry: Dependence on soil type and moisture profiles,” in *Proc. IEEE MicroRad*, Mar. 2006, pp. 171–175.

[10] J. P. Grant, A. A. V. de Griend, J.-P. Wigneron, K. Saleh, R. Panciera, and J. P. Walker, “Influence of forest cover fraction on L-band soil moisture retrievals from heterogeneous pixels using multi-angular observations,” *Remote Sens. Environ.*, vol. 114, no. 5, pp. 1026–1037, May 2010.

[11] M. Guglielmetti, M. Schwank, C. Matzler, C. Oberdorster, J. Vanderborght, and H. Fluhler, “FOSMEX: Forest soil moisture experiments with microwave radiometry,” *IEEE Trans. Geosci. Remote Sens.*, vol. 46, no. 3, pp. 727–735, Mar. 2008.

[12] N. Zhang, J. Shi, G. Sun, Z. Guo, and L. Chai, “Assessment of boreal forest biomass using L-band radiometer SMOS data,” in *Proc. IEEE Int. Geosci. Remote Sens. Symp.*, Jul. 2011, pp. 1946–1949.

[13] E. G. Njoku and D. Entekhabi, “Passive microwave remote sensing of soil moisture,” *J. Hydrol.*, vol. 184, nos. 1–2, pp. 101–129, Oct. 1996.

[14] J. Shi, L. Jiang, L. Zhang, K.-S. Chen, J.-P. Wigneron, and A. Chanzy, “A parameterized multifrequency-polarization surface emission model,” *IEEE Trans. Geosci. Remote Sens.*, vol. 43, no. 12, pp. 2831–2841, Dec. 2005.

[15] C. A. Laymon, W. L. Crosson, T. J. Jackson, A. Manu, and T. D. Tsegaye, “Ground-based passive microwave remote sensing observations of soil moisture at S-band and L-band with insight into measurement accuracy,” *IEEE Trans. Geosci. Remote Sens.*, vol. 39, no. 9, pp. 1844–1858, Sep. 2001.

[16] E. G. Njoku and J.-A. Kong, “Theory for passive microwave remote sensing of near-surface soil moisture,” *J. Geophys. Res.*, vol. 82, no. 20, pp. 3108–3118, Jul. 1977.

[17] E. G. Njoku, T. J. Jackson, V. Lakshmi, T. K. Chan, and S. V. Nghiem, “Soil moisture retrieval from AMSR-E,” *IEEE Trans. Geosci. Remote Sens.*, vol. 41, no. 2, pp. 215–229, Feb. 2003.

[18] S. Paloscia, P. Pampaloni, L. Chiarantini, P. Coppo, S. Gagliani, and G. Luzi, “ Multifrequency passive microwave remote sensing of soil moisture and roughness,” *Int. J. Remote Sens.*, vol. 14, no. 3, pp. 467–483, 1993.

[19] R. Panciera, O. Merlin, R. Young, and J. P. Walker, “The hydraprobe data acquisition system (HDAS): User guide,” Univ. Melbourne, Melbourne, Australia, Tech. Rep., Oct. 2006.

[20] M. Owe, R. de Jeu, and J. Walker, “A methodology for surface soil moisture and vegetation optical depth retrieval using the microwave polarization difference index,” *IEEE Trans. Geosci. Remote Sens.*, vol. 39, no. 8, pp. 1643–1654, Aug. 2001.